Radiation Detection Technology and Methods (2020) 4:263–268
https://doi.org/10.1007/s41605-020-00179-9

ORIGINAL PAPER

Study of muon tomographic imaging for high-*Z* material detection with a Micromegas-based tracking system

Cheng-Ming Liu[1] · Qun-Gang Wen[2] · Zhi-Yong Zhang[1] · Guang-Shun Huang[1]

Received: 27 February 2020 / Revised: 28 April 2020 / Accepted: 13 May 2020 / Published online: 29 May 2020

Abstract

Purpose To study the cosmic ray muon tomographic imaging of high-*Z* material with Micromegas-based tracking system.

Method A high-spatial-resolution tracking system was set up with the micro-mesh gaseous structure (Micromegas) detectors in order to study the muon tomographic imaging technique. Six layers of 90 mm × 90 mm one-dimensional readout Micromegas were used to construct a tracking system.

Result and conclusion The imaging test using some metallic bars was performed with cosmic ray muons. A two-dimensional imaging of the test object was presented with a newly proposed ratio algorithm. The result of this work shows that the ratio algorithm is well performed.

Keywords Muon tomography imaging · Micromegas detector · Ratio algorithm · High spatial resolution

Introduction

Muon imaging is a new technique developed to reconstruct images of volumes. According to the behaviors of muons in material, losing energy and absorbed in the material or changing direction after multiple Coulomb scattering, there are two different kinds of muon imaging: muon radiography and muon tomography imaging. A well-defined characteristic of this technique using cosmic ray muons is its non-invasiveness and economical value [1, 2]. Since its introduction in the 1950s [3], muon imaging has been under development for many purposes, such as observation of volcanic activity [1], nondestructive exploration of historical sites [4], monitoring nuclear waste containers [2], potential underground sites used for carbon sequestration [5] and detecting cargo containers at custom entrances [6]. This work is based on the muon tomography imaging.

Muons on Earth are the secondary particles that come from the extensive atmosphere shower of high-energy cosmic rays from space, with a flux about 1 cm^{-2} min^{-1} at sea level and an average energy of about 3 GeV. Thus, a high-efficiency and high-spatial-resolution tracing detector is required for timely imaging events. For instance, a GEANT4-based simulation shows that better than 200 μm spatial resolution is required for the imaging of a liter-sized (10 cm × 10 cm × 10 cm) uranium cores shielded on each of their six sides by 2.5 cm of material with lower *Z* (Al or Pb) which were placed at different coordinates within a muon tomography station (3 m × 3 m × 5 m) [6].

A micro-mesh gaseous structure (Micromegas) is a typical micro-pattern gas detector (MPGD), which has good spatial resolution of < 100 μm, and is easy to extend to large area [7, 8]. In this paper, a high-spatial-resolution tracking system consisting of 6 layers of one-dimensional readout Micromegas detectors is set up to study the muon imaging method for high-*Z* materials. The schematic design, detector and electronics, and data acquisition (DAQ) of the test system are demonstrated.

Three-dimensional algorithms like PoCA and MLEM reconstruct images and discriminate three cubes of different *Z* materials in a GEANT4-based simulation work [9, 10]. An image filtering technique is also applied to improve the

✉ Qun-Gang Wen
qungang@ahu.edu.cn

✉ Zhi-Yong Zhang
zhzhy@ustc.edu.cn

✉ Guang-Shun Huang
hgs@ustc.edu.cn

[1] State Key Laboratory of Particle Detection and Electronics, University of Science and Technology of China, Hefei 230026, China

[2] AnHui University, Hefei 230061, China

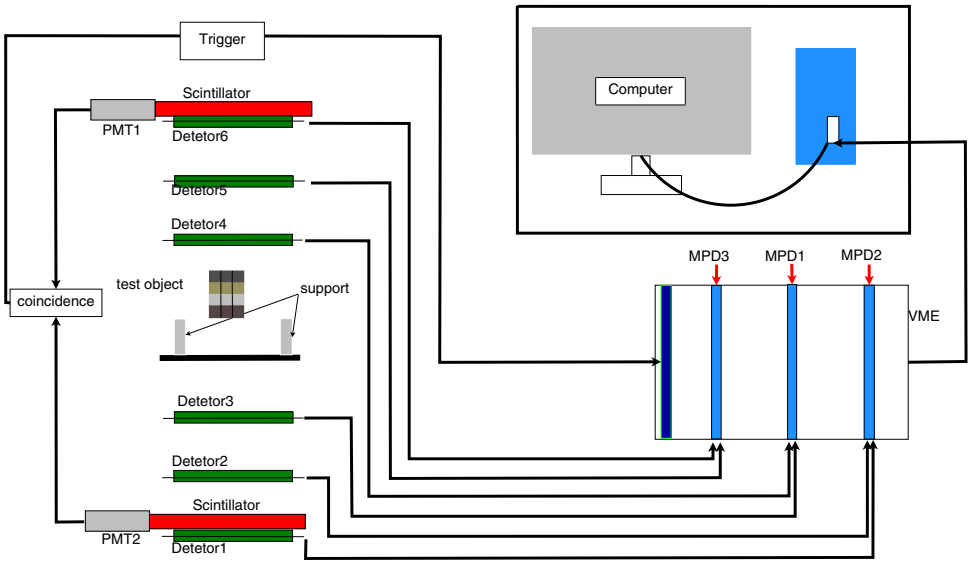

Fig. 1 Schematic design diagram for muon imaging study

performance of MLEM algorithm in simulation [11]. However, since most of the deflection angles of muons which are scattered by the nuclei of materials are small and the conventional analysis method used in tomography imaging is focusing on processing the large angle events, the utilization may be of low efficiency. So as to improve the utilization of the data including the small deflection angle events, the new ratio algorithm is introduced and applied to the real data. As a result, a two-dimensional imaging of a test object is finally obtained.

Tracking system

Schematic design

In this tracking system, two 150 mm × 150 mm scintillators are used to select effective events that penetrate the whole tracking detectors and provide trigger signals for the DAQ by coinciding their signals. Six layers of 90 mm × 90 mm one-dimensional readout Micromegas detectors are used to determine the tracks of incident and exiting muons from a test object. As shown in Fig. 1 , the detectors 4–6 are for the tracking of incident muons; detectors 1–3 are for exiting muons scattered by the nuclei of the test object. Signals of the Micromegas detectors are one-end readout by front-end electronics with APV25 ASICs [12] and digitized by multi-purpose digitizer (MPD) boards which are united to VME environments in data acquisition system.

The test object consists of four layers of different metallic bars including copper, iron, aluminum and tungsten, with the atomic mass A of 64, 56, 27 and 183, respectively. Each layer has the same three metallic bars with a size of 10 mm × 10 mm × 100 mm. In other words, it is a 30-mm-wide, 40-mm-high and 100-mm-long test object in total and is placed along the readout strips of Micromegas detectors.

Setup of the system

The Micromegas detectors are manufactured using the thermal bonding method [13, 14]. A resistive anode is employed to enhance the gas gain to higher than 10^4. The readout of detectors is designed as plane with 218 one-dimensional strips with a pitch of 412 μm and drift region of 5 mm; the gas mixture is 93% argon to 7% carbon dioxide. As a consequence, better than 150 μm spatial resolution and higher than 90% detection efficiency are obtained for the cosmic ray muons. As shown in Fig. 2, each Micromegas detector is installed in an aluminum plane, where a 100 mm × 100 mm hollow hole under the active area of detector is made to minimize the scattering materials in the tracker of muons. The direction orthogonal to the readout strips is defined as x-axis. When a charged particle triggers the detector, the cluster of avalanche may cover several strips with different signal amplitude; then, the center method is used to locate the X value of hit position.

The six detector planes are subsequently stacked to construct the tracking system as the schematic design mentioned above. Figure 3 shows the finished view of the installation of Micromegas detectors, and the test object is inserted in the middle of the tracking system. Finally, the whole system is calibrated and aligned with cosmic test, and effective muon events are collected for imaging analysis.

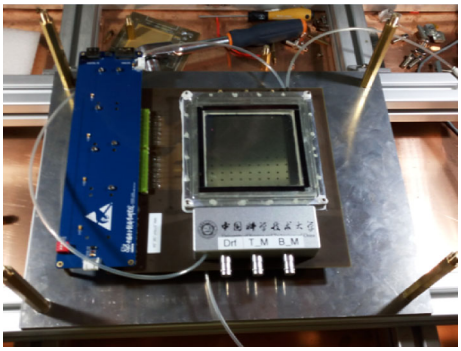

Fig. 2 Installation of the tracking system for a single detector

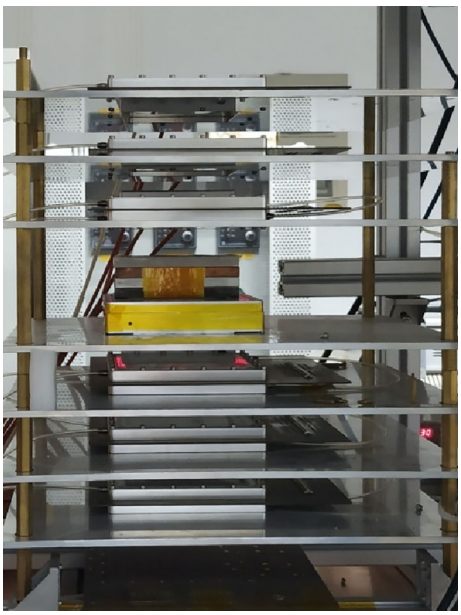

Fig. 3 Finished view of installation of the tracker detectors

Methods

Theory of muon scattering

In this experiment, a new ratio algorithm is proposed for imaging with the effective muon events, based on the idea of calculating the root mean square error value of the deflection angles of incoming and outgoing tracks of events in an exploration area. The deflection angle θ of muon passing through the material approximates a Gaussian distribution with a mean value of zero when considering the multi-Coulomb scattering as single scattering as Eq. 1 shows. Equation 2 gives an expression of the root mean square error σ_θ.

L is the length of a muon track in a certain material (air or test object). In this work, size of 33 mm × 33 mm is taken for the exploration area; considering the limited acceptance angle, the L value could be treated as a constant.

L_{rad} is the radiation length of the material, while the commonly used empirical formula is defined as Eq. 3, where Z and A are the atomic number and atomic mass of the substance, respectively, and β, c and p are the Lorentz parameters ($\beta \sim 1$), the velocity of light and the momentum of muons, respectively.

$$f(\theta) = \frac{1}{\sqrt{2\pi}\sigma_\theta} \exp\left(-\frac{\theta^2}{2\sigma_\theta^2}\right) \tag{1}$$

$$\sigma_\theta = \frac{13.6\ \text{MeV}}{\beta c p}\sqrt{\frac{L}{L_{\text{rad}}}}\left[1 + 0.038 \ln\left(\frac{L}{L_{\text{rad}}}\right)\right] \tag{2}$$

$$L_{\text{rad}} = \frac{716.4 \cdot A}{Z(Z+1)\ln(287/\sqrt{Z})}[\text{g/cm}^3] \tag{3}$$

The variables in Eq. 2 are momentum p and radiation length L_{rad}. In the case where momentum p is fixed value, as the atomic number Z increases the radiation length of the material decreases in Eq. 3, and the σ_θ increases accordingly in Eq. 2.

Defining H as Eq. 4, Eq. 2 can subsequently be written like Eq. 5.

$$H = \frac{13.6\ \text{MeV}}{\beta c}\sqrt{\frac{L}{L_{\text{rad}}}}\left[1 + 0.038 \ln\left(\frac{L}{L_{\text{rad}}}\right)\right] \tag{4}$$

$$\sigma_\theta^2 = \frac{1}{p^2}H^2 \tag{5}$$

For a distribution with a mean value of zero, its root mean square error can be obtained by fitting the experiment data into Eq. 6, where the θ_i represents the measured scattering angle of the number i of muon events in the data, and N the total number of events.

$$\sigma_\theta^2 = \frac{1}{N}\sum_{i=1}^{N}\theta_i^2 \tag{6}$$

Next, a test object which has a certain H value and whose N events can be divided into n groups according to the momentum of muons. For a group of muons in momentum bin p_i ($i = 1, 2\ldots n$), supposing there are k_i events with scattering angle $\theta_{i1}, \theta_{i2}\ldots \theta_{iki}$. A series of the root mean square errors can be obtained through Eqs. 5 and 6:

$$\sigma_1^2 = \frac{1}{k_1}\sum_{j=1}^{k_1}\theta_{1j}^2 = \frac{1}{p_1^2}H^2$$

$$\sigma_2^2 = \frac{1}{k_2}\sum_{j=1}^{k_2}\theta_{2j}^2 = \frac{1}{p_2^2}H^2$$

$\ldots$

$$\sigma_n^2 = \frac{1}{k_n}\sum_{j=1}^{k_n}\theta_{nj}^2 = \frac{1}{p_n^2}H^2$$

Rearranging these equations leads to Eq. 7, where the coefficient $\frac{k_i}{N}$ indicates the probability of muons in momentum bin p_i.

$$\sigma_\theta^2 = \frac{1}{N}\sum_{i=1}^{N}\theta_i^2 = \sum_{i=1}^{n}\frac{k_i}{N}\frac{1}{p_i^2}H^2 \tag{7}$$

when the amount of experimental data is sufficient, the momentum distribution can be considered to satisfy the natural distribution at sea level [15], such that the term $\sum_{i=1}^{n}\frac{k_i}{N}\frac{1}{p_i^2}$ can be considered as a constant value A which is indeed the average value $\left\langle\frac{1}{p^2}\right\rangle$ when N is large enough. Equation 7 consequently becomes:

$$\sigma_\theta^2 = \frac{1}{N}\sum_{i=1}^{N}\theta_i^2 = AH^2. \tag{8}$$

Compared to Eq. 5, the influence to root mean square error from the momentum of muons is negligible.

Ratio algorithm

An intuitive method for distinguishing different materials is to calculate the root mean square error of the muon scattering angles with Eq. 8, and it was named RMS error imaging method in this work. Due to the term which sums the square of the scattering angle, RMS error imaging method is sensitive to large angle events. In order to eliminate the effect of large angle and obtain good quality of imaging, it is necessary to constrain the angle range.

In another way, the so-called ratio algorithm was proposed in this work. Figure 4 shows the behaviors of muons passing through the test object. As mentioned in this paper, the deflection angles obey Gaussian distribution as Fig. 5 shows; the red line indicates the angle distribution of muons passing through the low atomic number Z material, while the blue line relates to the high-Z material.

As mentioned above, two tracks can be obtained when a muon event hit all the six detectors. The event will be considered as a straight track event if the deflection angle of these two reconstructed tracks is small due to the muon passed air or passed the test object without scattering; on the other hand, the event with large deflection angle will be considered as a scattered track event. The ratio value R is defined as Eq. 9

$$R = \frac{A_c}{A_0} \tag{9}$$

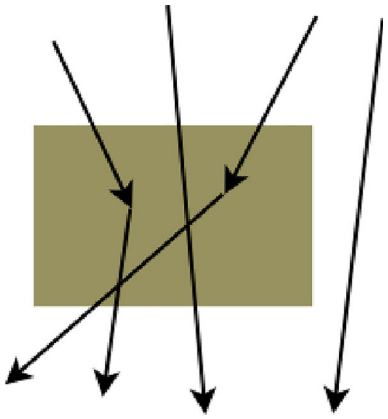

Fig. 4 Muon event pass through the test object

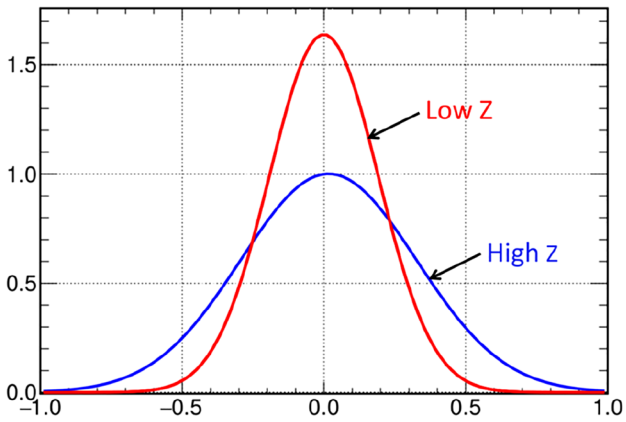

Fig. 5 Gaussian distribution of muon deflection angles in different materials

All of the events counted as A_0 that pass through the exploration area can be divided into two situations by studying the incoming and outgoing tracks: (1) For a straight track event, it will be recorded whether it passed the top margin or bottom margin of the exploration area. (2) For a scattered track event, it will be recorded only if the scattering point is in the exploration area, or it will be discarded. As for the events counted as A_c, which are the events with the deflection angles satisfy the selection criteria ($|\theta| < 1.6$ in this work) among the scattered track events.

The ratio value is actually the Gaussian function definite integral (or likelihood error function) of the root mean square error σ_θ, as shown in Eq. 10:

$$R(\theta_0) = \frac{1}{\sqrt{2\pi}\sigma_\theta}\int_{-\theta_0}^{\theta_0}\exp\left(-\frac{\theta^2}{2\sigma_\theta^2}\right)\mathrm{d}\theta \tag{10}$$

Obviously, for materials with different Z values, the higher the Z material has, the smaller the R value. In this way, different materials (air and test object in this work) can be distinguished. Furthermore, the R values could also be linked to the Z values if the tracks were precise enough.

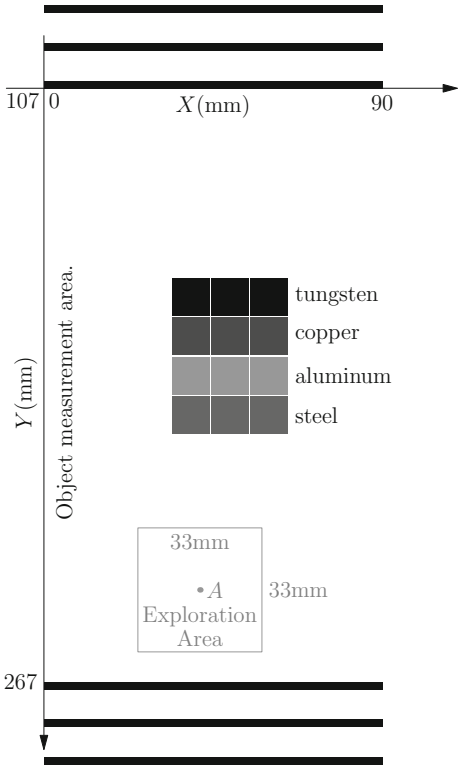

Fig. 6 Diagram of the description of the ratio algorithm

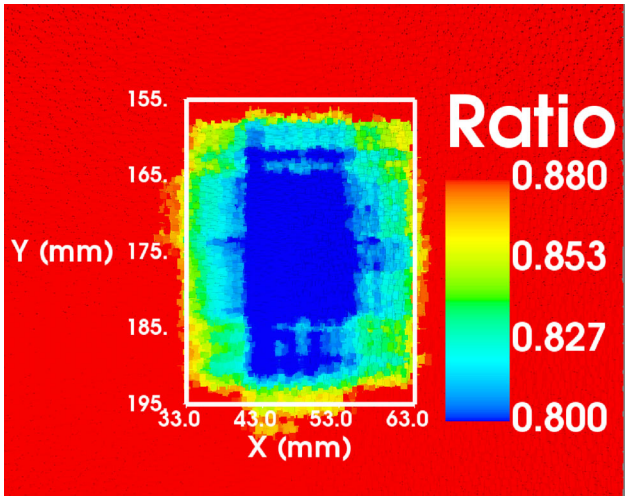

Fig. 7 Image of test object by cosmic ray muon tomography

Results

The ratio algorithm is proposed for eliminating the effects of large angle events. It is subsequently applied to experimental data. For detectors of the tracking system are one-dimensional, the x–y plane is focused in this work as shown in Fig. 6, which is the schematic diagram of the test system with the test object, and the positions along the y-axis are measurable; from top to bottom, the locations of six detectors are − 3.5 mm, 58.9 mm, 106.5 mm, 266.8 mm, 320.8 mm and 383.8 mm. When muons are scattered by a test object passing by all of the six detectors, the positions of the x-axis can be obtained through the detectors' readout. As a result, the two-dimensional positions of the exact scatter points are found. The incoming and outgoing x–y tracks can subsequently be reconstructed with a linear function fitting to the upper three points and lower three points, respectively. For imaging of the test object, ratios for all points in the measurement area are needed. As an example, the ratio at point A in Fig. 6 is calculated through the following steps:

- Take a square exploration area with a random point A as its center. Here, the exploration area is 33 mm × 33 mm.
- All events passing through the exploration area are counted as A_0, and events with scatter angles in a certain range ($|\theta| < 1.6°$ in this work) are counted as A_c
- Use Eq. 9 to get the ratio R.

All of the events counted as A_0 that pass through the exploration area can be divided into two situations by studying the incoming and outgoing tracks. (1) For a straight track, whether it passes the top margin or the bottom margin will be recorded; (2) for a scattered track, if the scattering point is in the exploration area it will be recorded; if not, then it will be discarded. Then these scattered tracks satisfy the selection criteria ($|\theta| < 1.6°$) that are counted as A_c. This shows that the ratio algorithm can make good use of these events which have scattering angle near 0°.

In order to ensure the unbiased R values, 500,000 points were selected randomly in the test object measurement area and the R values were calculated for all points. Consequently, a quantity field $R(x, y)$ (i.e., the R value with coordinates around point A) of the object measurement area is obtained. In this way, the image of cosmic ray muon tomography is visualized using ratios, as shown in Fig. 7. The rectangular box with coordinates shows the location and size of the test object. These points with ratio less than 0.800 are roughly formed into a rectangle. The reconstructed rectangle is smaller than the actual test object, but the reconstructed position is consistent with the actual position. Besides, these points with a ratio greater than 0.880 represent the air. The ratio value from 0.800 to 0.880 mainly occurs in the transition region between the test object (high-Z) and air (low Z). In this system, the reconstruction uses data from 793 effective muons detected in 1 day, with a detection flux about 10 cm^{-2} day^{-1}. The lower detection flux is due to removing the noised events caused by the detectors' performance. Improving detection flux will be very useful for rapid detection to some extent.

As mentioned above, constraining the scattered angle to suppress the effect of large angles is one feature of RMS error imaging method. These two algorithms are applied under

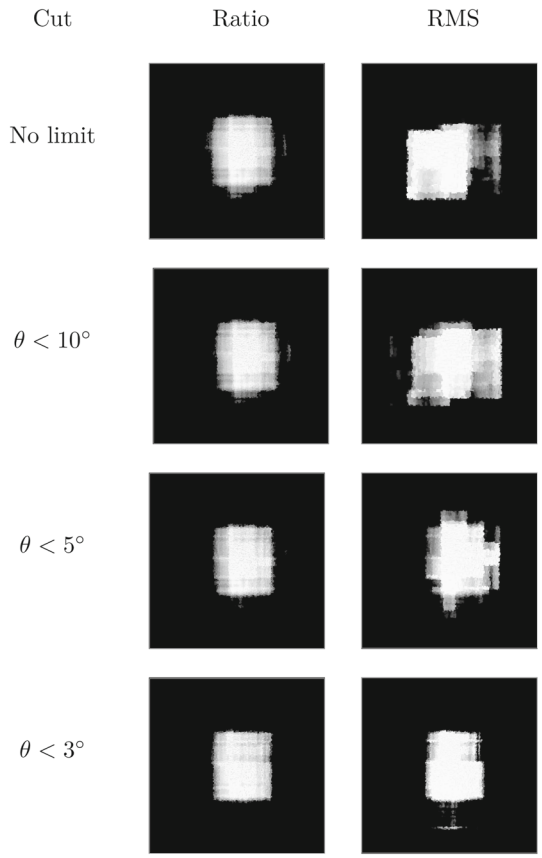

Fig. 8 Comparison of ratio and RMS error imaging method after the different angle limits

different scatter angle θ cuts for eliminating the large angle events, as shown in Fig. 8. It can be seen that more stringent angle cuts bring better imaging quality for RMS error imaging method, but less influence to ratio algorithm.

Discussion, future direction and conclusion

The muon tomography imaging is a very promising technique for non-invasiveness detecting with many potential applications such as detecting the shielded nuclear material in the cargo at the customs, monitoring the spent nuclear fuel and testing the cavity nondestructively in archeology or modern architectures. This work realized imaging with a tracking system based on Micromegas detectors, and a new proposed imaging algorithm named ratio algorithm which can make good use of events with scattering angles near 0° shows the effectiveness in the area of muon tomography imaging.

Development of this technique is ongoing. The focus of our work is on identifying different high-Z materials with ratio algorithm and on improving the performance of tracking system to achieve large acceptance and to get good quality data. In particular, two-dimensional readout detectors are under developing for new tracking system in order to achieve three-dimensional muon tomography imaging.

Acknowledgements This work was supported by the Program of National Natural Science Foundation of China Grant No. 11605197, the Fundamental Research Funds for the Central Universities, and the State Key Laboratory of Particle Detection and Electronics, SKLPDE-ZZ-201818, SKLPDE-KF-201912. This work was partially carried out at the USTC Center for Micro and Nanoscale Research and Fabrication, and we wish to thank Yu Wei for his help on the nanofabrication steps for germanium coating.

Compliance with ethical standards

Conflict of interest On behalf of all authors, the corresponding author states that there is no conflict of interest.

References

1. H. Tanaka et al., Development of an emulsion imaging system for cosmic-ray muon radiography to explore the internal structure of a volcano, Mt. Asama. Nucl. Instrum. Methods A **575**(3), 489–497 (2007)
2. G. Jonkmans et al., Nuclear waste imaging and spent fuel verification by muon tomography. Ann. Nucl. Energy **53**, 267–273 (2013)
3. E.P. George, Observations of the energy-spectrum of the cosmic radiation below ground. Nuc. Phys. **1**(8), 54–66 (1956)
4. K. Morishima et al., Discovery of a big void in Khufu's pyramid by observation of cosmic-ray muons. Nature **552**(7685), 386 (2017)
5. V.A. Kudryavtsev et al., Monitoring subsurface CO_2 emplacement and security of storage using muon tomography. Int. J. Greenh. Gas Control **11**, 21–24 (2012)
6. M. Hohlmann et al., GEANT4 simulation of a cosmic ray muon tomography system with micro-pattern gas detectors for the detection of high-Z materials. IEEE Trans. Nucl. Sci. **56**(3), 1356–1363 (2009)
7. Y. Giomataris et al., MICROMEGAS: a high-granularity position-sensitive gaseous detector for high particle-flux environments. Nucl. Instrum. Methods A **376**(1), 29–35 (1996)
8. M. Iodice, Micromegas detectors for the muon spectrometer upgrade of the ATLAS experiment. J. Instrum. **10**(02), C02026 (2015)
9. L.J. Schultz et al., Image reconstruction and material Z discrimination via cosmic ray muon radiography. Nucl. Instrum. Methods A **519**(3), 687–694 (2004)
10. L.J. Schultz et al., Statistical reconstruction for cosmic ray muon tomography. IEEE Trans. Image Process. **16**(8), 1985–1993 (2007)
11. S. Vanini et al., Muography of different structures using muon scattering and absorption algorithms. Philos. Trans. R. Soc. A **377**(2137), 20180051 (2019)
12. M.J. French et al., Design and results from the APV25, a deep submicron CMOS front-end chip for the CMS tracker. Nucl. Instrum. Methods A **466**(2), 359–365 (2001)
13. L. Guan et al., Micromegas prototypes with thermo-bond film separators. Chin. Phys. C **35**(2), 163–168 (2011)
14. Z. Zhang et al., Manufacture and performance of the thermal-bonding Micromegas prototype. J. Instrum. **9**(10), C10028 (2014)
15. S. Tsuji et al., Measurements of muons at sea level. J. Phys. G: Nucl. Part. Phys. **24**(9), 1805 (1998)